Hindawi Publishing Corporation
Mathematical Problems in Engineering
Volume 2010, Article ID 124148, 13 pages
doi:10.1155/2010/124148

Research Article

Influence of Asymmetric Mesh Stiffness on Dynamics of Spiral Bevel Gear Transmission System

Li Yinong, Li Guiyan, and Zheng Ling

The State Key Laboratory of Mechanical Transmission, Chongqing University, Chongqing 400044, China

Correspondence should be addressed to Li Yinong, ynli@cqu.edu.cn

Received 13 January 2010; Accepted 26 March 2010

Academic Editor: Carlo Cattani

An 8-DOF (degrees-of-freedom) nonlinear dynamic model of a spiral bevel gear pair which involves time-varying mesh stiffness, transmission error, backlash, and asymmetric mesh stiffness is established. The effect of the asymmetric mesh stiffness on vibration of spiral bevel gear transmission system is studied deliberately with numerical method. The results show that the mesh stiffness of drive side has more effect on dynamic response than those of the coast side. Only double-sided impact region is affected considerably by mesh stiffness of coast side while single-sided impact and no-impact regions are unchanged. In addition, the increase in the mesh stiffness of drive side tends to worsen the dynamic response of the transmission system especially for light-load case.

1. Introduction

Spiral bevel gear has been widely used in many power transmission systems due to its considerable technical advantages. Owing to backlash, time-varying mesh stiffness, and many other nonlinear factors, gear transmission system produces complex dynamic behavior which has aroused wide attention from scholars around the world. Since the first gear dynamic model was proposed by Tuplin in 1950s, considerable progress has been made in parallel axis gear dynamics [1–4]. However, the dynamics of a spiral bevel-geared system is lack of investigations when compared with the parallel system. Liangyu et al. [5] derived a twelve-degrees-of-freedom vibration model of a pair of Spiral bevel gears. Meanwhile an 8-DOF and a 2-DOF simplified model and a modified model with mesh error are given, which provides a theoretical foundation for studying dynamic response

of Spiral bevel gears. Gosselin et al. [6] proposed a general formula and applied it to analyze the load distribution and transmission error of spiral bevel gear pair and hypoid gear pair. Bibel et al. [7] studied the three-dimensional stress of a spiral bevel gear pair with finite element method. Fujii et al. [8] carried out analysis of dynamic behaviors of straight bevel-geared shaft supported on tapered roller and angular contact bearings, respectively, and then they measured the torsional and bending vibrations of the geared rotor and the vibrating displacement in the axial direction under a constant transmitted torque by using straight and skew bevel gears with a power circulating-type bevel-gear testing machine [9]. Xu et al. [10] analyzed the coupled lateral-torsional vibration behavior of the rotors with the engagement of spiral bevel gears by means of the transfer matrix method, which neglected the relationships of the generalized displacements between two bevel gears. Donley et al. [11] developed a dynamic model of a hypoid gear set for use infinite element analysis of gearing systems. In their gear mesh model, the mesh point and line-of-action are time invariant. Fang [12] developed a lumped parameter vibration model of a spiral bevel gear transmission to compute dynamic load and gear response. His mesh model is based on the classical gear mesh force equations that produce a simple unidirectional gear-mesh-coupling vector. Cheng and Lim [13] proposed a hypoid gear dynamic model based on exact gear geometry for analyzing gear mesh mechanism and applied the corresponding linear dynamic model to study the hypoid gear pair dynamics with transmission error excitation. In recent years, spiral bevel gear dynamics has gained extensive attention from many scholars and many relevant investigations have been published [14–17].

Unlike spur or helical gears, the mesh couplings in spiral bevel gears are not symmetric, due to the complex curvilinear features of the spiral bevel gear tooth geometry. That is, their mesh parameters for the drive and coast sides are very different. Most of the previous studies on the dynamics of spiral bevel gear transmissions focus on backlash and time-varying mesh stiffness, assuming symmetric mesh parameters for simplicity.

In this paper, we focus mainly on the dynamics of high-speed, precision spiral bevel gear pairs often used in automotive and aerospace power transmission systems. An 8-DOF nonlinear dynamic model of a spiral bevel gear pair which involves time-varying mesh stiffness, transmission error, backlash, and mesh stiffness asymmetry is proposed. Compared to mesh stiffness, the mesh damping with time-varying and asymmetric has less effect on dynamic response. Therefore, the study focuses on the effect of the asymmetric mesh stiffness on the vibration characteristics of spiral bevel gear transmission system, and the mesh damping parameter is assumed to be constant as in references [13, 14].

2. Dynamic Model

The proposed nonlinear dynamic model of a spiral bevel gear pair is shown in Figure 1. Three-dimensional Cartesian coordinate is set up, which uses the theoretical intersection of the two bevel gear axis for the origin. The two gear bodies are considered as rigid cone disks and bending rotation can be neglected for the bearing layout in Figure 1. Then the model includes transverse and torsion coordinates as shown in Figure 1.

The coordinate vector of the system can be expressed with $[X_1, Y_1, Z_1, \theta_{1x}, X_2, Y_2, Z_2, \theta_{2y}]^T$.

The normal dynamic load of pinion and its components along axis can be calculated as

$$\begin{aligned} F_n &= \overline{k}_h\left(\overline{\lambda}_n\right) f\left(\overline{\lambda}_n\right) + c_h \dot{\overline{\lambda}}_n, \\ F_x &= F_n\left(\sin\alpha_n \sin\delta_1 + \cos\alpha_n \sin\beta_m \cos\delta_1\right), \\ F_y &= -F_n\left(\sin\alpha_n \cos\delta_1 - \cos\alpha_n \sin\beta_m \sin\delta_1\right), \\ F_z &= -F_n \cos\alpha_n \cos\beta_m, \end{aligned} \tag{2.1}$$

$$\overline{k}_h\left(\overline{\lambda_n}\right) = \begin{cases} \overline{k}_{h1}, & \overline{\lambda_n} > \overline{b}, \\ 0, & -\overline{b} \le \overline{\lambda_n} \le \overline{b}, \\ \overline{k}_{h2}, & \overline{\lambda_n} < -\overline{b}, \end{cases}$$

$$\begin{aligned} \overline{k}_{h1} &= \overline{k}_{hm1} + \sum_{r=1}^{\infty} k_{har1} \cos\left(r\overline{\omega_h}\overline{t} + \phi_{hr1}\right), \\ \overline{k}_{h2} &= \overline{k}_{hm2} + \sum_{r=1}^{\infty} k_{har2} \cos\left(r\overline{\omega_h}\overline{t} + \phi_{hr2}\right), \end{aligned} \tag{2.2}$$

$$f\left(\overline{\lambda_n}\right) = \begin{cases} \overline{\lambda_n} - \overline{b}, & \overline{\lambda_n} > \overline{b}, \\ 0, & -\overline{b} \le \overline{\lambda_n} \le \overline{b}, \\ \overline{\lambda_n} + \overline{b}, & \overline{\lambda_n} < -\overline{b}, \end{cases}$$

where $\overline{k}_{h1}$, $\overline{k}_{h2}$—mesh stiffness of drive side and coast side, respectively; $\overline{\lambda}_n$—Dynamic transmission error; $\overline{k}_h(\overline{\lambda_n})$, $f(\overline{\lambda}_n)$—Nonlinear displacement function; c_h—Mesh damping coefficient; α_n—Normal surface pressure angle; δ_1—Pitch cone angle of the pinion; β_m—Helix angle at meshing point; $\overline{k}_{hm1}$, $\overline{k}_{hm2}$—Mean mesh stiffness of drive side and coast side, respectively; k_{har1}, k_{har2}—Fourier series coefficients; $\overline{b}$—Half of the gear backlash.

Dynamic transmission error can be defined with

$$\overline{\lambda}_n = (-X_1 + X_2)a_1 + (Y_1 - Y_2)a_2 + \left(Z_1 - Z_2 + r_{m1}\theta_{1x} - r_{m2}\theta_{2y}\right)a_3 + \overline{e}\left(\overline{t}\right), \tag{2.3}$$

where

$$\begin{aligned} a_1 &= \sin\alpha_n \sin\delta_1 + \cos\alpha_n \sin\beta_m \cos\delta_1, \\ a_2 &= \sin\alpha_n \cos\delta_1 - \cos\alpha_n \sin\beta_m \sin\delta_1, \\ a_3 &= \cos\alpha_n \cos\beta_m, \end{aligned} \tag{2.4}$$

$\overline{e}(\overline{t})$ is the static transmission error on normal direction of meshing surface. It can be expressed in a Fourier series form: $\overline{e}(\overline{t}) = \sum_{r=1}^{\infty} \overline{e}_r \sin(r\overline{\omega_h}\overline{t} + \phi_{er})$, where r_{m1}, r_{m2}—mean radius at meshing point; $\overline{e}_r$—amplitude of the r-order harmonic; ϕ_{er}—phase angle of the r-order harmonic.

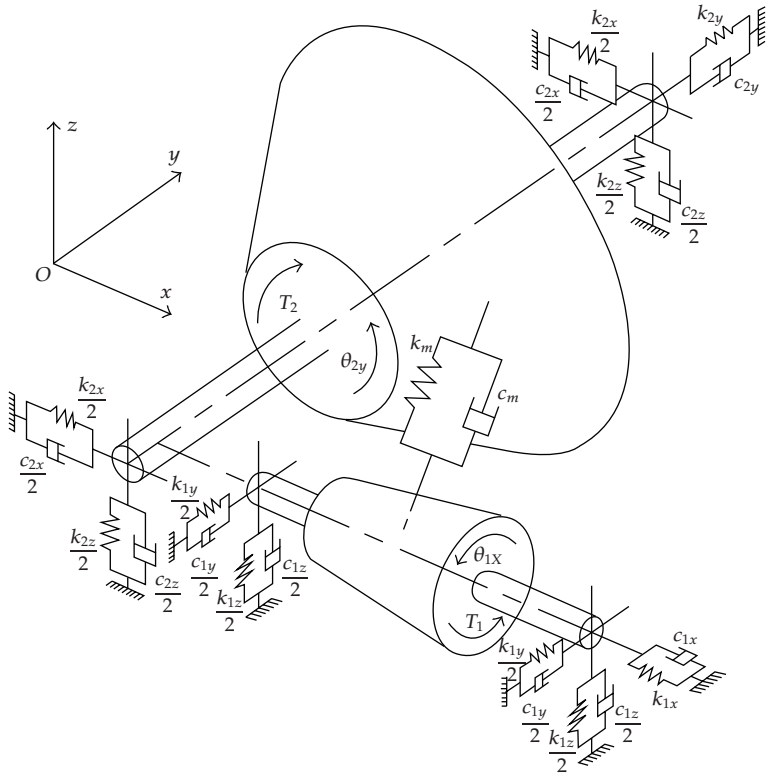

Figure 1: Dynamic model of a spiral bevel gear pair.

The equations of the dynamic model can be described as

$$\begin{aligned}
m_1\ddot{X}_1 + C_{1x}\dot{X}_1 + K_{1x}X_1 &= F_x,\\
m_1\ddot{Y}_1 + C_{1y}\dot{Y}_1 + K_{1y}Y_1 &= F_y,\\
m_1\ddot{Z}_1 + C_{1z}\dot{Z}_1 + K_{1z}Z_1 &= F_z,\\
I_{1x}\ddot{\theta}_{1x} &= T_1 + F_z r_{m1},\\
m_2\ddot{X}_2 + C_{2x}\dot{X}_2 + K_{2x}X_2 &= -F_x,\\
m_2\ddot{Y}_2 + C_{2y}\dot{Y}_2 + K_{2x}Y_2 &= -F_y,\\
m_2\ddot{Z}_2 + C_{2z}\dot{Z}_2 + K_{2z}Z_2 &= -F_z,\\
I_{2y}\ddot{\theta}_{2y} &= -T_2 - F_z r_{m2},
\end{aligned} \tag{2.5}$$

$$T_1 = T_{1m} + T_{1v}, \qquad T_2 = T_{2m}, \tag{2.6}$$

where m_1, m_2—Mass of pinion and gear, respectively; I_{1x}, I_{2y}—Mass moments of inertias of pinion and gear, respectively; K_{ij}, C_{ij}—Bearing stiffness and damping along the three coordinate axis, respectively; T_1, T_2—Load torques on pinion and gear, respectively; T_{1m}, T_{2m}—Mean load torques on pinion and gear, respectively; T_{1v}—Ripple torque on pinion.

Using $\overline{\lambda}_n$ as a new freedom degree, the two rigid-body rotation equations of the original model can be changed into a single one:

$$\begin{aligned}
&m_e a_1 \ddot{X}_1 - m_e a_2 \ddot{Y}_1 - m_e a_3 \ddot{Z}_1 - m_e a_1 \ddot{X}_2 + m_e a_2 \ddot{Y}_2 + m_e a_3 \ddot{Z}_2 \\
&+m_e \ddot{\overline{\lambda}}_n + c_h a_3^2 \dot{\overline{\lambda}}_n + \overline{k}_h\left(\overline{\lambda}_n\right) a_3^2 f\left(\overline{\lambda}_n\right) = a_3(F_{1m} + F_{1v}) + m_e \ddot{\overline{e}}_n\left(\overline{t}\right), \\
&m_e = \frac{I_{1x} I_{2y}}{\left(I_{1x} r_{m2}^2 + I_{2y} r_{m1}^2\right)}, \\
&F_{1m} = \frac{T_{1m}}{r_{m1}} = \frac{T_{2m}}{r_{m2}}, \\
&F_{1v} = \frac{T_{1v} r_{m1} m_e}{I_{1x}} = \sum_{r=1}^{\infty} F_r \cos\left(r\omega_{T1} t + \phi_{T1r}\right),
\end{aligned} \tag{2.7}$$

where m_e—Equivalent mass of the gear pair; F_{1v}, F_{1m}—Ripple and mean force on pinion, respectively.

Next, introducing the parameters

$$x_i = \frac{X_i}{l}, \quad y_i = \frac{Y_i}{l}, \quad z_i = \frac{Z_i}{l}, \quad b = \frac{\overline{b}}{l},$$

$$\lambda_n = \frac{\overline{\lambda}_n}{l}, \ \omega_n = \sqrt{\frac{k_{hm}}{m_e}}, \quad \omega_{ij} = \sqrt{\frac{k_{ij}}{m_i}},$$

$$\varsigma_{ij} = \frac{c_{ij}}{(2m_i\omega_n)}, \quad \varsigma_{ih} = \frac{c_h}{(2m_i\omega_n)},$$

$$k_{ij} = \frac{\omega_{ij}^2}{\omega_n^2}, \quad k_{ih} = \frac{\overline{k}_h\left(\overline{\lambda}_n\right)}{\left(m_i\omega_n^2\right)},$$

$$t = \omega_n \bar{t}, \quad \omega_h = \frac{\overline{\omega_h}}{\omega_n}, \quad \omega_T = \frac{\overline{\omega}_T}{\omega_n},$$

$$k_{hm} = \frac{\left(\overline{k}_{hm1} + \overline{k}_{hm2}\right)}{2},$$

$$g_1 = \frac{\overline{k}_{h1}}{k_{hm}} = k_{hm1} + \sum_{r=1}^{\infty} k_{hr1} \cos\left(r\omega_h t + \phi_{hr1}\right),$$

$$g_2 = \frac{\overline{k}_{h2}}{k_{hm}} = k_{hm2} + \sum_{r=1}^{\infty} k_{hr2} \cos\left(r\omega_h t + \phi_{hr2}\right),$$

$$g(\lambda_n) = \begin{cases} g_1, & \lambda_n > b, \\ 0, & -b \le \lambda_n \le b, \\ g_2, & \lambda_n < -b, \end{cases}$$

$$f(\lambda_n) = \begin{cases} \lambda_n - b, & \lambda_n > b, \\ 0, & -b \le \lambda_n \le b, \\ \lambda_n + b, & \lambda_n < -b, \end{cases}$$

$$f_{1m} = \frac{F_{1m}}{m_e l \omega_n^2}, \quad f_{1v} = \frac{F_{1v}}{m_e l \omega_n^2},$$

$$f_e = \sum_{r=1}^{\infty} F_{hr} (r\omega_h)^2 \cos\left(r\omega_h t + \phi_{er}\right), \tag{2.8}$$

where $i = 1, 2$; $j = x, y, z$.

The dimensionless form of (2.5) can be obtained as

$$\ddot{x}_1 + 2\varsigma_{1x}\dot{x}_1 + k_{1x}x_1 - 2a_1\varsigma_{1h}\dot{\lambda}_n - a_1 k_{1h} f(\lambda_n) = 0,$$

$$\ddot{y}_1 + 2\varsigma_{1y}\dot{y}_1 + k_{1y}y_1 + 2a_2\varsigma_{1h}\dot{\lambda}_n + a_2 k_{1h} f(\lambda_n) = 0,$$

$$\ddot{z}_1 + 2\varsigma_{1z}\dot{z}_1 + k_{1z}z_1 + 2a_3\varsigma_{1h}\dot{\lambda}_n + a_3 k_{1h} f(\lambda_n) = 0,$$

$$\ddot{x}_2 + 2\varsigma_{2x}\dot{x}_2 + k_{2x}x_2 + 2a_2\varsigma_{2h}\dot{\lambda}_n + a_2 k_{2h} f(\lambda_n) = 0,$$

$$\ddot{y}_2 + 2\varsigma_{2y}\dot{y}_2 + k_{2y}y_2 - 2a_2\varsigma_{2h}\dot{\lambda}_n - a_2 k_{2h} f(\lambda_n) = 0,$$

$$\ddot{z}_2 + 2\varsigma_{2z}\dot{z}_2 + k_{2z}z_2 - 2a_3\varsigma_{2h}\dot{\lambda}_n - a_3 k_{2h} f(\lambda_n) = 0,$$

$$a_1\ddot{x}_1 - a_2\ddot{y}_1 - a_3\ddot{z}_1 - a_1\ddot{x}_2 + a_2\ddot{y}_2 + a_3\ddot{z}_2 + \ddot{\lambda}_n + 2a_3^2\varsigma_h\dot{\lambda}_n + a_3^2 g(\lambda_n) f(\lambda_n) = a_3 f_{1m} + a_3 f_{1v} + f_e. \tag{2.9}$$

3. Numerical Results

As there is no analytical method existing for (2.9), the equation is solved by applying the explicit Runge-Kutta integration routine with variable step that is generally applicable to strong nonlinear equation. The effect of tooth mesh stiffness asymmetry on dynamic response of spiral bevel gear system for both light and heavy loads is studied here. For subsequent numerical study, the baseline data used are

$$Z_1 = 36, \quad Z_2 = 40, \quad \alpha_n = 20^\circ, \quad \beta_m = 35^\circ, \quad \overline{b} = 35\,\mu\text{m}. \tag{3.1}$$

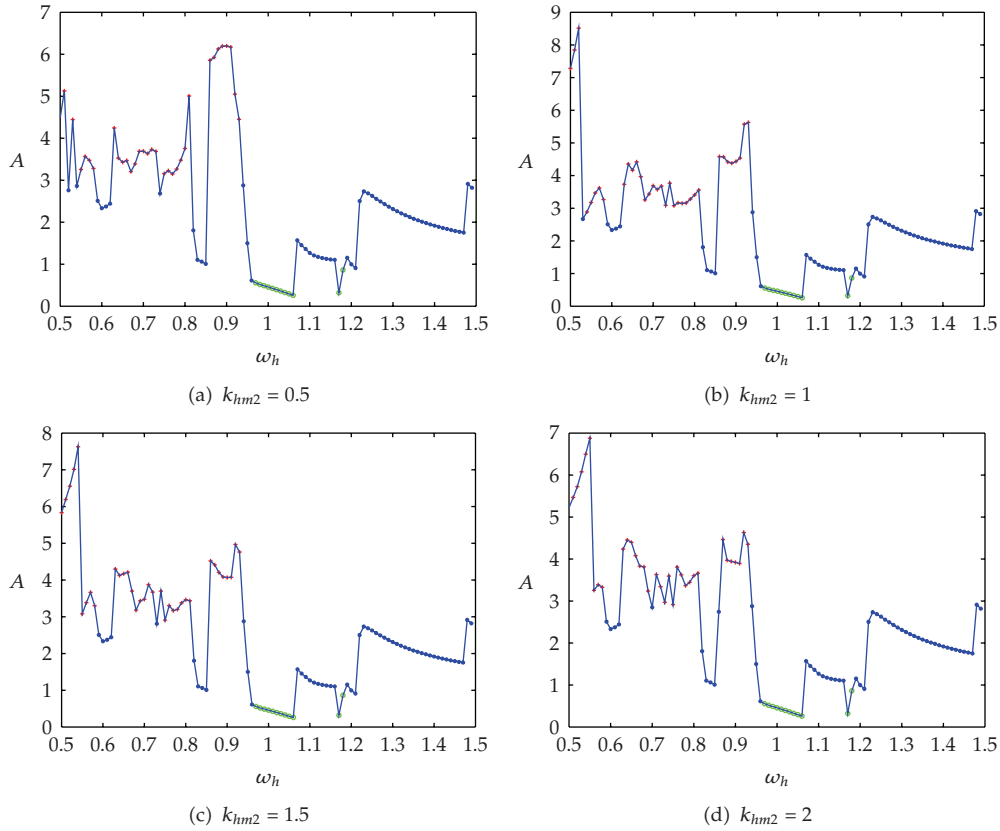

Figure 2: Effect of mean mesh stiffness of coast side for lightly loaded case. ∗—single-sided impact ∘—no impact +—double-sided impact.

In this part, it is focused on effect of mean mesh stiffness k_{hm1}, k_{hm2}, assuming that $k_{hr1} = k_{hr1}$, $\phi_{hr1} = \phi_{hr2}$ for simplicity.

3.1. Effect of Mesh Stiffness Asymmetry for Lightly Loaded Case

Dimensionless dynamic parameters set in the system are as follows:

$$\begin{gathered}
\varsigma_{ij} = 0.01, \qquad \varsigma_{ih} = 0.0125, \qquad \varsigma_{ih} = 0.0125, \\
k_{ih} = 0.25, \qquad k_{hr1} = k_{hr2} = 0.2, \\
\phi_{hr1} = \phi_{hr2} = 0, \\
f_{1m} = 0.25, \qquad f_{1v} = 0 \quad \omega_h = 0.7, \\
f_e = 0.5\omega_h^2 \cos\omega_h t, \quad i = 1, 2, \ j = x, y, z.
\end{gathered} \tag{3.2}$$

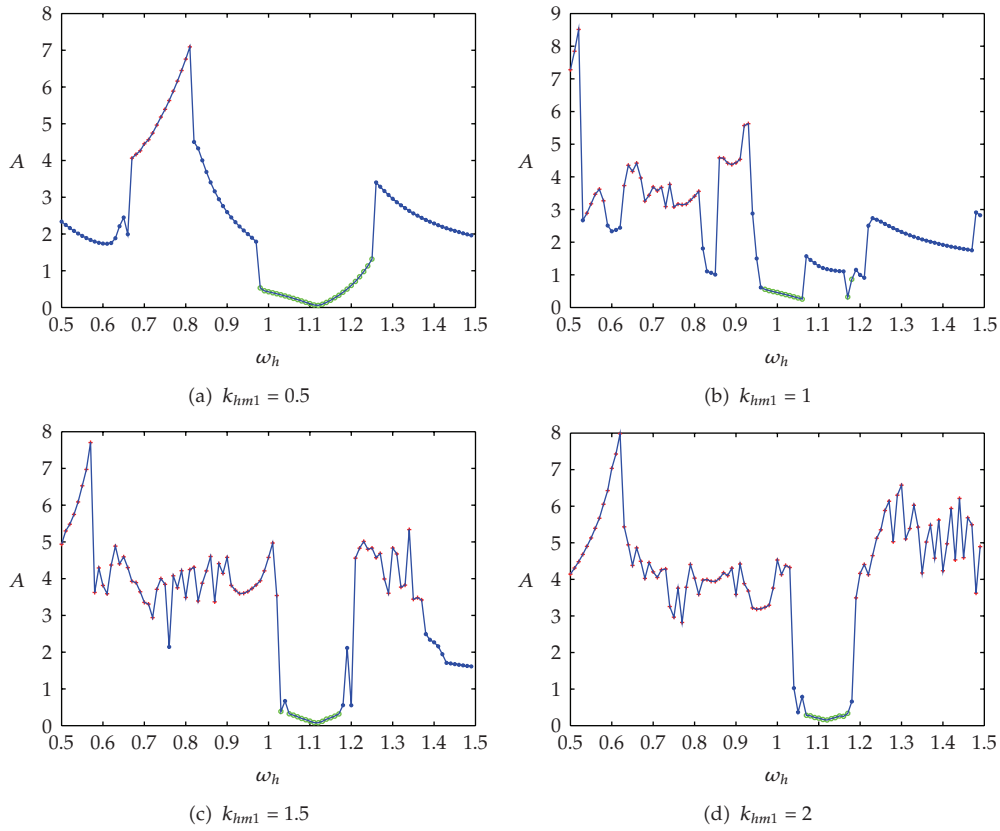

Figure 3: Effect of mean mesh stiffness of drive side for lightly loaded case. ∗—single-sided impact ∘—no impact +—double-sided impact.

The effect of the mean mesh stiffness of coast side on dynamic response for lightly loaded case is shown in Figure 2. The horizontal axis represents excitation frequency ω_h and the vertical axis represents peak-peak value of the dynamic transmission error A. As shown in Figure 2(a), when $k_{hm2} = 0.5$, single-sided impact response and double-sided impact response alternate in the low-frequency regions. And the max of A occurs at $\omega_h = 0.9$. In the region $\omega_h \in [0.96, 1.06]$, there are no impact responses, and the gear pair running smoothly as k_{hm2} is increased to 1 in Figure 2(b); the max of A 8.5 moves to the frequency $\omega_h = 0.52$. The dynamic response in no-impact and single-sided impact regions $\omega_h \in [0.96, 1.5]$ keeps unchanged. When k_{hm2} is increased further to 1.5 and 2, the peak-peak value A in double-sided impact region changes obviously while the location and vibration response of single-sided impact and no-impact regions are nearly unchanged. The above results show that the mesh stiffness of coast side only affects double-sided tooth impact region.

Figure 3 shows the effect of mean mesh stiffness of drive side for lightly loaded case. It can be seen from Figure 3(a) that double-sided impacts dominate the range $\omega_h \in [0.67, 0.79]$. And four response jump discontinuities can be seen at frequency $\omega_h = 0.67, 0.79, 0.97, 1.25$. It can be observed that response jump discontinuities appear at these frequencies. As k_{hm1} is increased to 1, it can be observed that more double-sided impacts appear and the location of each impact region shifts obviously. As k_{hm1} is further increased to 1.5 and 2, both response

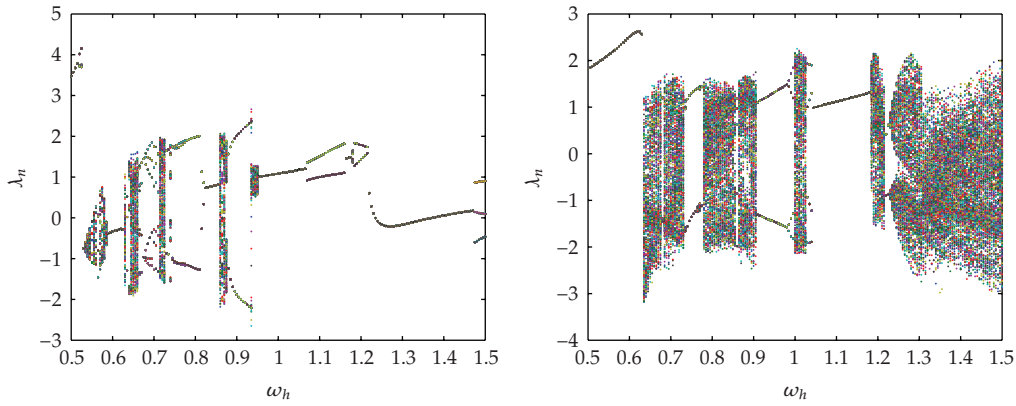

(a) $k_{hm1} = 1$ (b) $k_{hm1} = 2$

Figure 4: Bifurcation diagram for lightly loaded case.

jumps and single-sided impacts increased considerably, and response in the whole excitation frequency areas changes significantly. As can be seen in Figure 3(c), except the two narrow bands $\omega_h \in [1.03, 1.17]$ and $\omega_h \in [1.36, 1.5]$, the rest excitation frequencies are all double-sided impact regions. When $k_{hm1} = 2$, width of double-sided tooth impact region is further increased.

To further explain the effect of the mean mesh stiffness of drive side on dynamic response, bifurcation diagram is introduced in Figure 4. For the current light-load case, it can be observed that, as k_{hm1} is increased from 1 to 2, chaotic motion regions increase considerably. From above observations, it can be concluded that the mesh stiffness of drive side affects dynamic response greatly in the whole excitation frequency region. Furthermore, the increase of drive side mesh stiffness tends to worsen dynamic response.

3.2. *Effect of Mesh Stiffness Asymmetry for Heavily Loaded Case*

Dimensionless dynamic parameters set in this part are as follows:

$$\begin{gathered} \varsigma_{ij} = 0.01, \quad \varsigma_{ih} = 0.0125, \quad \varsigma_{ih} = 0.0125, \quad k_{ih} = 0.25, \quad k_{hr1} = k_{hr2} = 0.2, \\ \phi_{hr1} = \phi_{hr2} = 0, \quad f_{1m} = 1, \quad f_{1v} = 0, \quad f_e = 0.5\omega_h^2 \cos \omega_h t, \\ i = 1, 2, \quad j = x, y, z. \end{gathered} \tag{3.3}$$

When $k_{hm1} = 1$, the effect of k_{hm2} for heavy-load case is shown in Figure 5. No-impact region $\omega_h \in [0.74, 1.18]$ is far wider than double-sided impact region $\omega_h \in [0.5, 0.61]$ in Figure 5(a). And the max of $A = 15.9$ which comes at $\omega_h = 0.52$ is much larger than that of 6 for light-load case. There are three single-sided impact regions $\omega_h \in [0.62, 0.73]$, $\omega_h \in [1.19, 1.27]$, and $\omega_h \in [1.32, 1.5]$, and little response jump can be seen. As k_{hm2} is increased to 1, dynamic response in double-sided impact region changes greatly while responses in single-sided impact and no-impact regions remain the same. And the max of A is increased to 24. As k_{hm2} is increased further to 1.5 and 2, only double-sided impact region is affected. The results show that double-sided impact region becomes obviously narrower

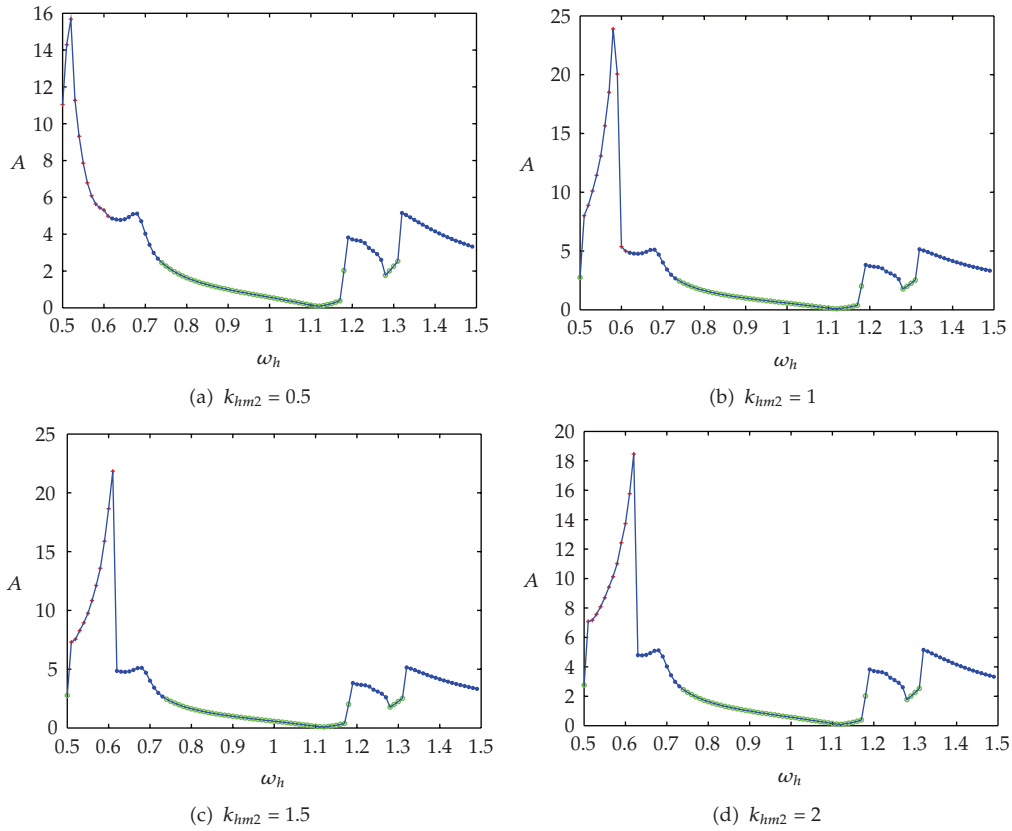

Figure 5: Effect of mean mesh stiffness of coast side for heavily loaded case. ∗—single-sided impact ∘—no impact +—double-sided impact.

and response jumps diminish considerably for heavily loaded case. Although the peak-peak value of dynamic transmission error in double-sided impact region is larger than that of light-load case, response jump discontinuities and double-sided tooth impacts for heavily loaded case are far fewer. As light-load condition, only double-sided impact region is affected considerably by mesh stiffness of coast side. This is because k_{hm2} only takes effect for double-sided impact condition.

Figure 6 shows dynamic response for different mean mesh stiffness of drive side while leaving mean mesh stiffness of coast side unchanged. In Figure 6(a), there are three no-impact regions $\omega_h \in [0.98, 1.33]$, $\omega_h \in [0.57, 0.79]$, and $\omega_h \in [1.44, 1.5]$, one double-sided impact region $\omega_h \in [0.8, 0.91]$, and three response jump frequencies $\omega_h = 0.8$, $\omega_h = 0.91$, and $\omega_h = 0.97$. The max of $A = 32$ occurs at $\omega_h = 0.92$. As k_{hm1} is increased to 1, no-impact regions are reduced to two $\omega_h \in [0.74, 1.18]$ and $\omega_h \in [1.28, 1.31]$, and the location of each impact region changes significantly. For $k_{hm1} = 1.5$ in Figure 6(c), the number of double-sided impact region is increased to two $\omega_h \in [0.57, 0.76]$ and $\omega_h \in [1.31, 1.41]$, and more response jumps appear. When k_{hm1} is increased to 2, double-sided impact region becomes wider and response in double-sided impact region takes significant changes from Figure 6(c).

Figure 7 shows response bifurcation for different k_{hm1}, while k_{hm2} is fixed to 1. For $k_{hm1} = 1$ in Figure 7(a), no chaotic motion can be seen. However, as k_{hm1} is increased to 2,

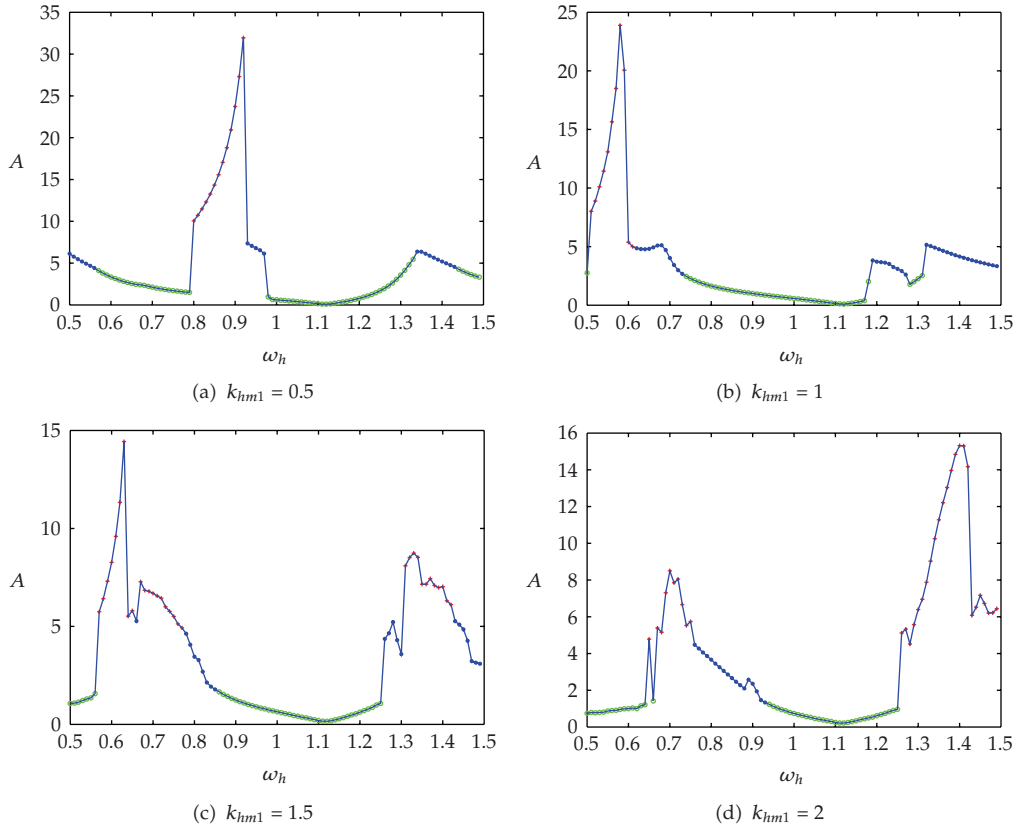

Figure 6: Effect of mean mesh stiffness of drive side for heavily loaded case. ∗—single-sided impact ∘—no impact +—double-sided impact.

there are two obvious chaotic motion areas. Comparing with Figure 4, it can be seen that chaotic motion areas diminish considerably in Figure 7. From these results we can conclude that mesh stiffness of drive side also affects dynamic response greatly for heavy-load case. In addition, the increase of k_{hm1} will worsen the dynamic response of the system especially for light-load case. Compared with light-load condition, the degree of gear backlash nonlinearity is lower for heavy-load case. This is because mesh force under heavy-load condition is large and hence mesh teeth are difficult to separate.

4. Conclusions

A nonlinear dynamic model of a spiral bevel gear pair which involves time-varying mesh stiffness, transmission error, backlash, and mesh stiffness asymmetry is proposed. The effect of tooth mesh stiffness asymmetry on vibration of spiral bevel gear transmission system is studied deliberately. Some important conclusions are obtained.

Firstly, the mesh stiffness for drive side has more effect on dynamic response than those of the coast side. Only double-sided impact region is affected considerably by mesh stiffness of coast side while single-sided impact and no-impact regions are unchanged.

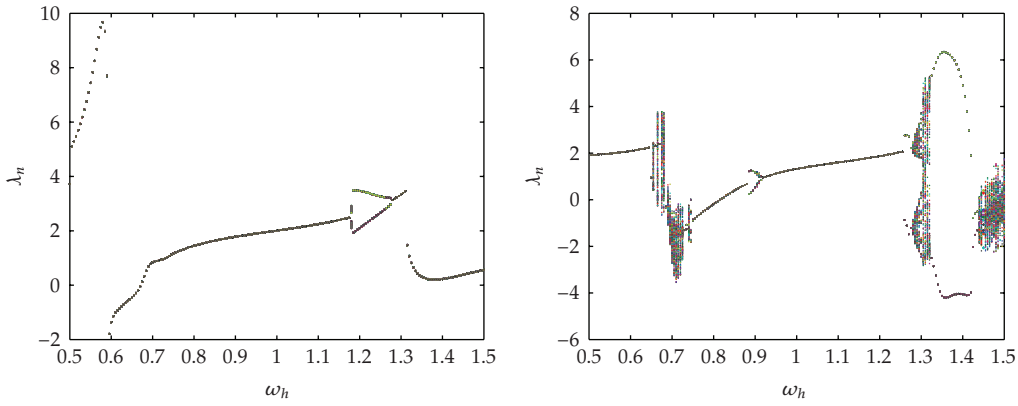

(a) $k_{hm1} = 1$ (b) $k_{hm1} = 2$

Figure 7: Bifurcation diagram for heavily loaded case.

Secondly, the dynamic response of the system is very sensitive to mesh stiffness of drive side. The change of mesh stiffness of drive side will affect response in the whole excitation frequency areas. Furthermore, the increase of drive side mesh stiffness tends to worsen dynamic response especially for lightly loaded case.

Thirdly, the vibration characteristic for heavily loaded case is far better than that for lightly loaded case. And the mesh stiffness asymmetry affects the dynamic response more compared with heavy-load case.

Acknowledgments

This paper is supported by National Natural Science Foundation of China (Grant no. 50875270), Key Scientific Projects of Ministry of Education of China (Grant no. 108108) and Natural Science Foundation of Chongqing (CSTC, 2008BA6025).

References

[1] L. Runfang and W. Jianjun, *Dynamics of Geared System—Vibration, Impact, Noise*, Science Publishing House, Beijing, China, 1997.

[2] A. Kahraman and R. Singh, "Non-linear dynamics of a spur gear pair," *Journal of Sound and Vibration*, vol. 142, no. 1, pp. 49–75, 1990.

[3] A. Kahraman and R. Singh, "Non-linear dynamics of a geared rotor-bearing system with multiple clearances," *Journal of Sound and Vibration*, vol. 144, no. 3, pp. 469–506, 1991.

[4] W. Jianjun, L. Qihan, and L. Runfang, "Research advances for nonlinear vibration of gear transmission system," *Advances In Mechanics*, vol. 35, no. 1, pp. 37–51, 2005 (Chinese).

[5] C. Liangyu, C. Chunyuan,, and E. Zhongkai, "A vibration model spiral bevel gears," *Journal of Northeast University of Technology*, vol. 14, no. 2, pp. 146–149, 1993 (Chinese).

[6] C. Gosselin, L. Cloutier, and Q. D. Nguyen, "A general formulation for the calculation of the load sharing and transmission error under load of spiral bevel and hypoid gears," *Mechanism and Machine Theory*, vol. 30, no. 3, pp. 433–450, 1995.

[7] G. D. Bibel, A. Kumar, S. Reddy, and R. Handschuh, "Contact stress analysis of spiral bevel gears using finite element analysis," *Journal of Mechanical Design*, vol. 117, no. 2 A, pp. 235–240, 1995.

[8] M. Fujii, Y. Nagasaki, M. Nohara, and Y. Terauchi, "Effect of bearing on dynamic behaviors of straight bevel gear," *Transactions of the Japan Society of Mechanical Engineers. Part C*, vol. 61, no. 581, pp. 234–238, 1995 (Japanese).

[9] M. Fujii, Y. Nagasaki, and M. Nohara, "Differences in dynamic behavior between straight and skew bevel gears," *Transactions of the Japan Society of Mechanical Engineers. Part C*, vol. 63, no. 613, pp. 3229–3234, 1997 (Japanese).

[10] l. Z. Xu, M. Zhao, P. Z. Ren, and W. D. Chai, "Method for analyzing the vibration behavior of rotor with the engagement of spiral bevel gears," *Mechanical Science and Technology*, vol. 16, pp. 668—673, 1997.

[11] M. G. Donley, T. C. Lim, and G. C. Steyer, "Dynamic analysis of automotive gearing systems," *Journal of Passenger Cars*, vol. 101, no. 905, pp. 77–87, 1992.

[12] Z. D. Fang, "Dynamic analysis of spiral bevel gears in assembly," in *Proceedings of the International Gearing Conference*, vol. 43, pp. 389–392, Newcastle, UK, 1994.

[13] Y. Cheng and T. C. Lim, "Vibration analysis of hypoid transmissions applying an exact geometry-based gear mesh theory," *Journal of Sound and Vibration*, vol. 240, no. 3, pp. 519–543, 2001.

[14] J. Wang, T. C. Lim, and M. Li, "Dynamics of a hypoid gear pair considering the effects of time-varying mesh parameters and backlash nonlinearity," *Journal of Sound and Vibration*, vol. 308, no. 1-2, pp. 302–329, 2007.

[15] S. Wang, Y. Shen, and H. Dong, "Nonlinear dynamical characteristics of a spiral bevel gear system with backlash and time-varying stiffness," *Chinese Journal of Mechanical Engineering*, vol. 39, no. 2, pp. 28–32, 2003.

[16] L. Wang, Y. Huang, R. Li, and T. Lin, "Study on nonlinear vibration characteristics of spiral bevel transmission system," *China Mechanical Engineering*, vol. 18, no. 3, pp. 260–264, 2007 (Chinese).

[17] M. Li and H. Y. Hu, "Dynamic analysis of a spiral bevel-geared rotor-bearing system," *Journal of Sound and Vibration*, vol. 259, no. 3, pp. 605–624, 2003.